Piezo1 calcium flickers localize to hotspots of cellular traction forces

Kyle Ellefsen* [1], Alice Chang* [2], Jamison L. Nourse* [3,6], Jesse R. Holt [3], Janahan Arulmoli [4,6], Armen Mekhdjian [2], Lisa A. Flanagan [4,5,6], Alexander R. Dunn [2], Ian Parker [1,3], Medha M. Pathak [3,6,†]

[1] Department of Neurobiology & Behavior, UC Irvine, Irvine, CA.
[2] Department of Chemical Engineering, Stanford University, Stanford, CA.
[3] Department of Physiology & Biophysics, UC Irvine, Irvine, CA.
[4] Department of Biomedical Engineering, UC Irvine, Irvine, CA.
[5] Department of Neurology, UC Irvine, Irvine, CA.
[6] Sue and Bill Gross Stem Cell Research Center, UC Irvine, Irvine, CA.

* Equal contribution
† Correspondence: medhap@uci.edu

Keywords: Piezo1, traction forces, micropatterned cells, molecular tension sensor, Piezo1 diffusion, Ca^{2+} signaling, cellular force maps, Ca^{2+} flickers

ABSTRACT

Piezo channels transduce mechanical stimuli into electrical and chemical signals to powerfully influence development, homeostasis, and regeneration. Due to their location in the plasma membrane, they are positioned to transduce both external mechanical forces in the environment as well as internal forces generated by cells. While much is known about how Piezo1 responds to externally-applied mechanical forces, its response to cell-generated forces that are vital for cellular and organismal physiology is poorly understood. Here we show that Ca^{2+} flickers generated by endogenous Piezo1 channel activity in human neural stem/progenitor cells and human fibroblasts are stimulated by proximal piconewton to nanonewton scale actomyosin-based cellular traction forces. Further, although Piezo1 channels diffuse readily in the plasma membrane and are widely distributed across the cell, flicker activity is enriched in spatially constrained regions at force-producing adhesions. We propose that Piezo1-mediated Ca^{2+} flickers allow spatial segregation of mechanotransduction events within cells, and that Piezo1 diffusion allows a few channel molecules to efficiently respond to transient and localized mechanical stimuli throughout the entire cell surface.

INTRODUCTION

Cells have the ability to detect and generate mechanical forces, and integrate this mechanical information with genetic and chemical cues to shape organismal morphology, growth, and homeostasis. Mechanical forces are transduced into biochemical signals by specialized proteins. Among these, mechanically-activated ion channels provide unique features: sub-millisecond conversion of mechanical stimuli into electrical and chemical signals, high sensitivity, large dynamic range, spatial coding of mechanical stimuli, and the ability for temporal filtering of repetitive stimuli (Nourse and Pathak 2017).

Piezo channels were recently identified as a new family of excitatory mechanically-activated channels (Coste et al. 2010, 2012). Due to their permeability to Ca^{2+} and other cations, Piezo channel activity generates electrical as well as chemical signals in response to mechanical stimuli, allowing them to regulate a wide variety of cellular processes. Indeed, Piezo1 has emerged as an important player in physiological processes as diverse as vascular development (J. Li et al. 2014; Ranade et al. 2014), neural stem cell differentiation (Pathak et al. 2014), bladder mechanosensation (Miyamoto et al. 2014), erythrocyte volume regulation (Cahalan et al. 2015), cell migration (Hung et al. 2016; C. Li et al. 2015; McHugh et al. 2012), vascular smooth muscle remodeling (Retailleau et al. 2015), blood pressure regulation (S. Wang et al. 2016) and exercise physiology (Rode et al. 2017). The global knockout of Piezo1 is embryonic lethal (Ranade et al. 2014), and mutations in the channel have been linked to diseases such as dehydrated hereditary stomatocytosis (Albuisson et al. 2013; Andolfo et al. 2013; Bae et al. 2013; Zarychanski et al.

2012), colorectal adenomatous polyposis (Spier et al. 2016), and generalized lymphatic dysplasia (Fotiou et al. 2015; Lukacs et al. 2015). Thus, understanding how Piezo1 functions is critical for understanding its diverse physiological roles.

Studies on the Piezo1 channel have largely focused on transduction of mechanical forces from outside the cell to inside the cell (Cox et al. 2016; Coste et al. 2010; J. Li et al. 2014; Ranade et al. 2014; Syeda et al. 2016; Gottlieb, Bae, and Sachs 2012; Poole et al. 2014). However, cells also actively generate intracellular mechanical forces. The plasma membrane, as the interface between the cell's intra- and extracellular environments, is subject to mechanical forces from both inside and outside the cell. Thus, Piezo1 in the plasma membrane is situated to respond to intracellular and extracellular mechanical forces. Most studies of Piezo1 have utilized patch clamp assays that, by their design, evaluate Piezo1 response to externally-applied mechanical stimuli. In whole cell patch clamp, a mechanical stimulus is applied by indenting the cell with a glass probe while the electrical response is recorded from the entire cell. In cell-attached patch clamp, mechanical stimuli are administered by negative suction pulses applied to the back of the patch pipette while the electrical activity is measured from channels in the microscopic patch of membrane in the pipette.

Both patch clamp configurations drastically affect the native environment of Piezo1. In whole-cell patch clamp, cellular contents are dialyzed by the large reservoir of solution in the patch pipette, confounding the study of channel activation and modulation by the cytoskeleton and soluble intracellular molecules. In cell-attached patch clamp, the intracellular contents are retained, but the gigaseal connection between the membrane and glass pipette exerts an intense mechanical stress on the membrane patch (Suchyna, Markin, and Sachs 2009). This is sufficient to drive a large fraction of Piezo1 channels into inactivation (Lewis and Grandl 2015), resulting in an artificially higher activation threshold compared to physiological conditions.

An alternative non-perturbing method to monitor activation of Piezo1 channels involves imaging Ca^{2+} flux through the channel rather than electrophysiological measurements of ionic current (Pathak et al. 2014; Gaub and Müller 2017). Using this approach in human neural stem/progenitor cells (hNSPCs), we previously found that Piezo1 underlies discrete, local, and transient Ca^{2+} microdomains or "flickers" in the absence of externally-applied mechanical forces; activity that underlies the mechanosensitive lineage choice of hNSPCs during differentiation (Pathak et al. 2014). These Piezo1 flickers are reversibly inhibited by pharmacological inhibition of Myosin II, an actin-based molecular motor critical for cellular force generation (Pathak et al. 2014).

Here we examine the relationship between Piezo1 activity and Myosin II-based traction forces that cells use for probing the stiffness of their extracellular matrix. We image Piezo1 flickers at submicron-scale spatial resolution and millisecond-scale temporal resolution in conjunction with visualizing tdTomato-tagged Piezo1 in live cells and with techniques to manipulate (Singhvi et al. 1994; Chen et al. 1997) and measure cell-generated actomyosin forces (Stabley et al. 2011; Morimatsu et al. 2013; Grashoff et al. 2010). We find that although Piezo1 channels appear to diffuse readily in the plasma membrane and are widely distributed across the cell, flicker activity is enriched in regions in which cells exert mechanical traction forces on their substrate. In light of recent evidence demonstrating that membrane tension gates Piezo1 (Cox et al. 2016; Syeda et al. 2016; Lewis and Grandl 2015), our studies suggest that cellular traction forces generate transient, local increases in membrane tension that activates Piezo1 within spatial microdomains. We further propose that Piezo1 channel mobility allows a small number of channels to explore a wide array of mechanical microdomains, and hence respond to both unpredictable external forces as well as to hotspots of cell-generated traction forces.

RESULTS

Super-resolution localization of Piezo1 flickers

We previously reported Piezo1 flickers at the cell-substrate interface by imaging Ca^{2+} influx through the channel with total internal reflection fluorescence microscopy (TIRFM) (Pathak et al. 2014). The greater signal-to-noise ratio afforded by TIRFM allowed us to detect small signals arising from the activity of endogenously expressed channels at the cell-substrate interface. In that study we detected

Piezo1 events by manually examining acquired movies, drawing a region of interest (ROI) around visible events, and plotting the average intensity inside ROIs over time. To determine the spatial dynamics of native Piezo1 flickers with higher fidelity, we developed a technique for automated localization of Piezo1 flickers at super-resolution levels. This approach is an improved version of our algorithm for automated detection and quantitation of local Ca^{2+} signals (Ellefsen et al. 2014), implemented as a plugin for the general purpose image processing software Flika (http://flika-org.github.io). The algorithm developed herein uses a clustering method (Rodriguez and Laio 2014) to group suprathreshold pixels into Ca^{2+} events, improving the unbiased detection and segregation of signals.

Figure 1 shows an implementation of the algorithm applied to Piezo1 flickers recorded from hNSPCs (see Methods for further details). As in our previous study, we imaged Piezo1 flickers by imaging Ca^{2+} influx through the channel using TIRFM (Fig. 1A). The raw movie is processed to produce a F/F_0 ratio movie (Fig. 1B) which is then spatially and temporally filtered to increase the signal-to-noise ratio of the signals of interest. The processed movie is passed through the clustering algorithm for event detection. Once events are detected, a 2-dimensional (2D) Gaussian curve is fit to every event in the movie to determine the localization of each flicker event with super-resolution precision. Figure 1C shows the output of the algorithm for a single, representative flicker event after pre-processing steps (Fig. 1C, top and middle) and after the super-resolution localization of the event by Gaussian fitting (Fig. 1C, bottom). The peak of this 2D Gaussian (red arrow, Fig. 1C bottom) identifies the center of the calcium event with subpixel accuracy. Assuming the diffusion of Ca^{2+} is radially symmetric, this gives the location of an individual ion channel or the 'center of mass' of a group of ion channels underlying the event. These flicker localizations are overlaid on an image of the cells (Fig. 1D) to produce a cellular map of active Piezo1 channels. The extracted signals can be analyzed to determine peak amplitude, temporal dynamics, and frequency of signals at a specific site (Fig. 1E). This technique made it possible for us to examine the spatial localization of Piezo1 activity in relation to cellular traction forces.

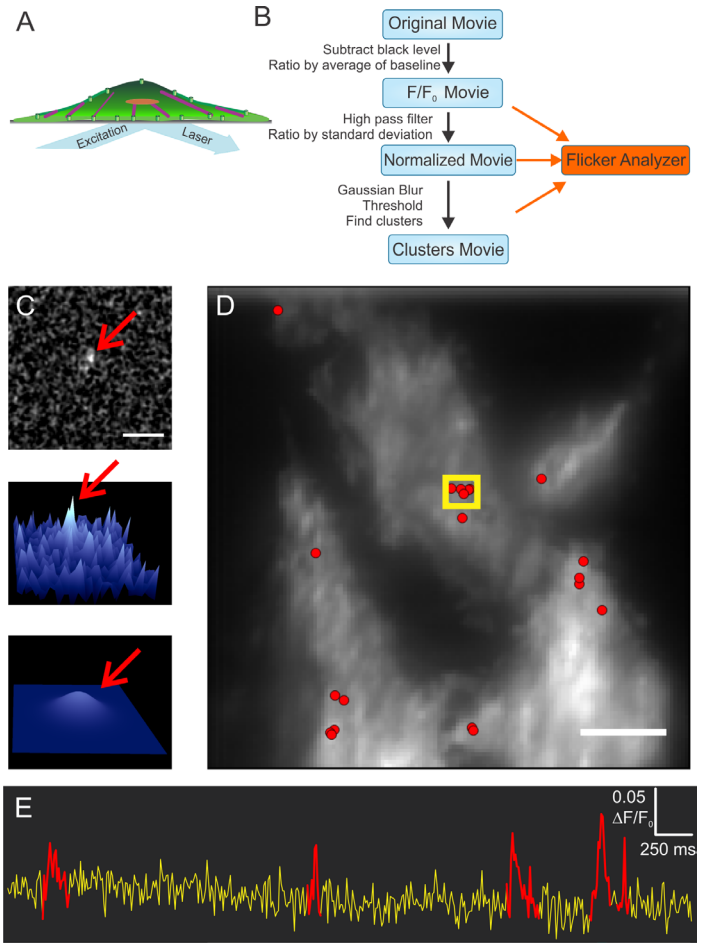

Figure 1. Automated detection and super-resolution analysis of Piezo1 flickers. A. Piezo1 flickers are acquired by Ca^{2+} imaging with Total Internal Reflection Fluorescence Microscopy (TIRFM). **B.** Flowchart of the algorithm. The original movie is processed to subtract camera black level and then divided by the average of the first ~100 frames to produce a F/F_0 ratio movie. The ratioed movie is spatially and temporally filtered to increase the signal-to-noise ratio. A clustering algorithm groups supra-threshold pixels into flicker events. **C.** For every event detected, a 2D Gaussian fit to the fluorescence intensity identifies with sub-pixel accuracy the centroid of the fluorescence, and therefore of the ion channel(s) producing the Ca^{2+} signal. Representative images of a 200 µm x 200 µm region showing a processed, filtered Piezo1 flicker event (top, red arrow), a 3D representation of the event (middle) and the Gaussian fit to the event (bottom). Arrow in bottom panel marks the peak of the Gaussian profile that identifies with sub-pixel accuracy the location of the centroid of the Ca^{2+} flicker. **D.** Ficker localizations (red dots) overlaid on an image of an hNSPC to map sites of Piezo1 activity. **E.** Flicker activity from the region of interest marked in D plotted over time as fluorescence ratio changes ($\Delta F/F_0$). Identified flicker events are highlighted in red. Scale bars = 50 µm.

Piezo1 flickers are enriched at regions predicted to have high traction forces

To relate Piezo1 flicker activity to cellular traction forces, we mapped Piezo1 activity in cells gen-

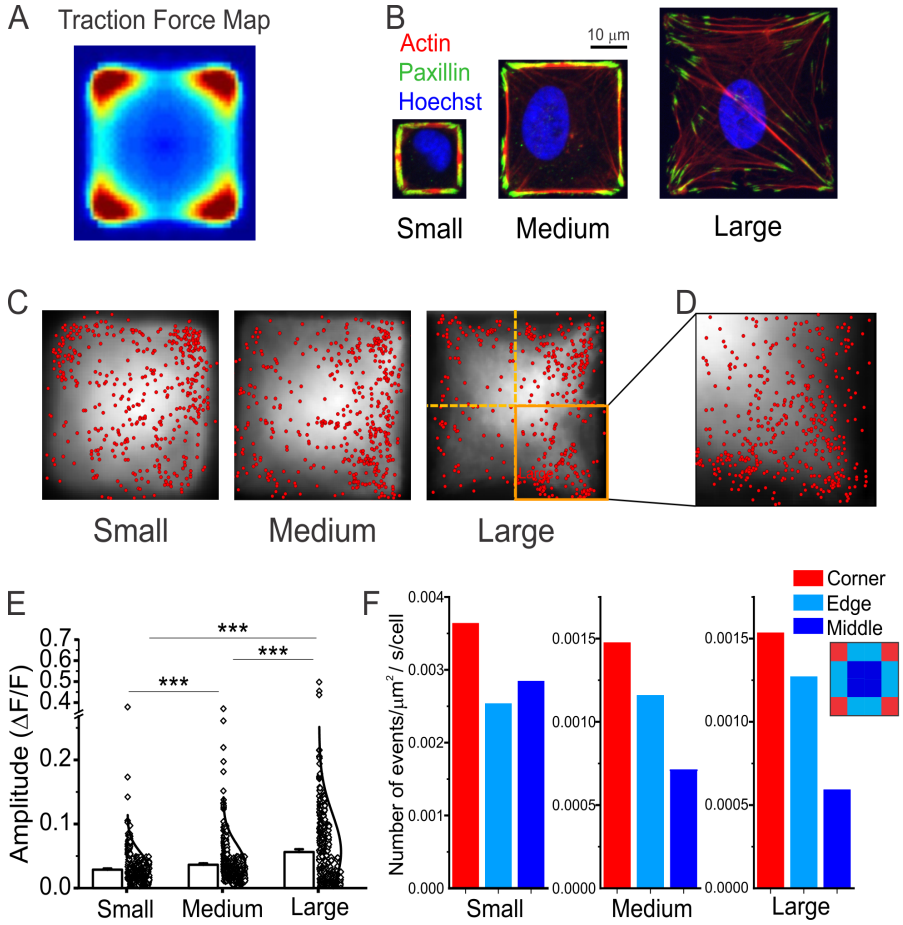

Figure 2. Piezo1 flickers are enriched in regions of cells predicted to have higher traction forces. A. Cells constrained to adopt a square shape on a patterned substrate generate the largest traction forces at the corners (red), lower levels of forces at the edges (cyan) and lowest traction forces in the middle of the cell. The image is reproduced from Holt *et al.* 2012 under CC BY-NC-SA 3.0 license. **B.** hNSPCs seeded on square fibronectin islands yield a single square cell per island. Images are representative confocal slices stained for the actin cytoskeleton (phalloidin, red), the focal adhesion zone protein, paxillin (anti-paxillin antibody, green) and the nucleus (Hoechst, blue). Note the larger number of actin stress fibers terminating in focal adhesions for cell adhering to larger islands. Island sizes used: Small, 300 µm^2; Medium 1024 µm^2; Large, 2025 µm^2. **C.** Localizations of Piezo1 flickers within cells seeded on Small, Medium and Large islands. Each panel shows an image of a Cal520-loaded hNSPC, with an overlay of individual Piezo1 flicker localizations from multiple cells (red dots). The panels are shown scaled to the same size for ease of comparison. Total numbers of events represented in panels C, D, E are: Small, 453 events from 7 cells; Medium, 476 events from 7 cells; Large, 426 events from 4 cells. Data was acquired with an exposure time of 5ms (200 Hz frame rate).**D.** Flicker locations from all four quadrants of Large size mapped on to a single quadrant of a Cal520-loaded hNSPC. **E**. Bar and Data plot of flicker amplitudes for events from cells adhering to Small, Medium and Large islands. Each dot represents an individual Piezo1 flicker event and bars denote the mean of all events for the specified cell size. Piezo1 flickers show greater amplitudes ($\Delta F/F_0$) in cells seeded on large islands. *** denotes $p < 0.001$by two-sample t-test. **F.** Frequencies of Piezo1 flickers in corner regions (red area in square inset), edge regions (light blue, square inset), middle regions (dark blue, square inset) of cells grown on Small, Medium and Large islands. Data are expressed as the number of events per µm^2 per second per cell.

erating known patterns of traction forces using the well-established effect of cell geometry on traction forces: cell shape determines *where* forces are generated and cell size determines *how much* force is generated (Parker et al. 2002; Tan et al. 2003; N. Wang et al. 2002; Théry 2010). We controlled the shape and size of hNSPCs -- and therefore the spatial pattern and magnitude of their cellular traction forces -- using substrate micropatterning (Singhvi et al. 1994; Chen et al. 1997; Théry 2010) and examined Piezo1 activity maps in these micropatterned cells. To do so, glass coverslips were patterned with islands of fibronectin of pre-determined shapes and sizes. Upon seeding, cells bind to fibronectin via cellular integrins and take up the geometry of the island. We selected the shape of our substrate islands based on previous traction force measurements in micropatterned cells (Parker et al. 2002; Tan et al. 2003; N. Wang et al. 2002; Holt et al. 2012), which show that in cells constrained to a square shape, traction forces are highest at the

vertices, moderately high at edges, and minimal in the center of the cell (Fig. 2A). Moreover, as the size of the square island is increased, the magnitude of traction force increases (Tan et al. 2003; Théry 2010). This robust dependence of traction forces on the shape and size of micropatterned square cells allowed us to ask whether the location and magnitude of Piezo1 flickers in square cells also shows a similar dependence on cell shape and size.

We seeded hNSPCs on glass substrates in square shapes of three different sizes (Small 17.3 μm x 17.3 μm= 300 μm^2, Medium 32 μm x 32 μm = 1024 μm^2, Large 45 μm x 45 μm = 2025 μm^2). We confirmed that micropatterned hNSPCs exhibited the shape and cytoskeletal organization expected of this geometry. We visualized actin filaments in fixed micropatterned hNSPCs with fluorescent-labeled phalloidin, focal adhesion zones with an anti-Paxillin antibody, and cell nuclei with Hoechst dye (Fig. 2B). As expected, each square island was occupied by a single cell. Cells on larger islands displayed greater numbers of, and longer, actin stress fibers, terminating in paxillin-rich focal adhesions that were concentrated in corner regions. Cells on Large islands displayed a network of actin stress fibers across the cell, while cells on Small islands showed actin accumulated primarily along the edges, as previously observed in other cell types for this specific set of square patterns (Dupont et al. 2011).

Having determined that hNSPCs showed the expected cellular architecture when confined to square islands, we next imaged Piezo1 flickers in live cells adhering to Small, Medium, and Large square islands and extracted their amplitudes and locations (Fig. 2C-F). Flicker amplitudes were greater in larger cells (Fig. 2E), which are known to generate larger traction forces. To determine the location of Piezo1 activity relative to the predicted traction force distribution, we determined the occurrence of flickers in three regions of the cell: Corner, Middle, and Edge regions normalized for area, as depicted in Fig. 2F. If active sites were randomly distributed, we would expect an equal occurrence of flickers in Corner, Middle, and Edge regions. However, we observed that for all three cell sizes, Corner regions showed more flickers per unit area per second (Fig. 2F). As cell spread area increased, the distribution of events shifted from the Middle region to Corner and Edge regions (Fig. 2C, 2D, 2F). Overall, our measurements show that Piezo1 flicker amplitudes scale with cell size, and that Piezo1 flickers are enriched in regions expected to have higher traction forces.

Measuring Piezo1 flickers and traction forces in the same cell

Enrichment of Piezo1 flickers in regions of micropatterned hNSPCs predicted to have higher traction forces motivated us to measure traction forces and Piezo1 flickers in the same cell. We used a Förster resonance energy transfer (FRET)-based molecular tension sensor (MTS) to measure cellular traction forces (Chang et al. 2016). The MTS is comprised of an elastic peptide which separates a covalently-bound FRET pair (Fig. 3A). The N-terminus of the sensor is covalently attached to a functionalized glass coverslip to produce a carpet of sensors. The C-terminus of the MTS has a fibronectin fragment to which cells bind via integrins. Cells seeded on to the sensor-coated glass coverslip adhere to the substrate via the MTS. Traction forces generated by the cell are communicated to the MTS via integrin-MTS attachments: these forces cause extension of the peptide spring, leading to a separation of the FRET pair and therefore a reduction in FRET efficiency. The FRET donor and acceptor channels are simultaneously imaged, yielding FRET index maps, calculated by dividing the acceptor intensity over the sum of donor and acceptor intensities. A high FRET index indicates low traction force and a low FRET index indicates high traction force. The FRET index maps can be converted to FRET efficiency maps to allow extraction of quantitative values for force based on the FRET-force response of the elastic peptide (Morimatsu et al. 2015; Grashoff et al. 2010), see Methods for details). Thus, imaging the donor and acceptor fluorophores allows production of a quantitative, high-resolution traction force map of the cell. Compatibility of these sensors with TIRFM-based Ca^{2+} imaging allowed us to measure and correlate cellular traction forces and Piezo1 activity in the same cell, a measurement that would be difficult using conventional traction force microscopy.

We seeded hNSPCs onto coverslips functionalized with the MTS, allowed the cells to attach and spread for 1-2 hours, then loaded them with the Ca^{2+} indicator Cal-520 AM. We imaged force maps followed by Piezo1 activity maps from the same cell (Fig. 3B, C). Overlaying the two maps demonstrated that Piezo1 flickers occurred in regions of the cell that displayed high traction forces (Fig. 3C). To

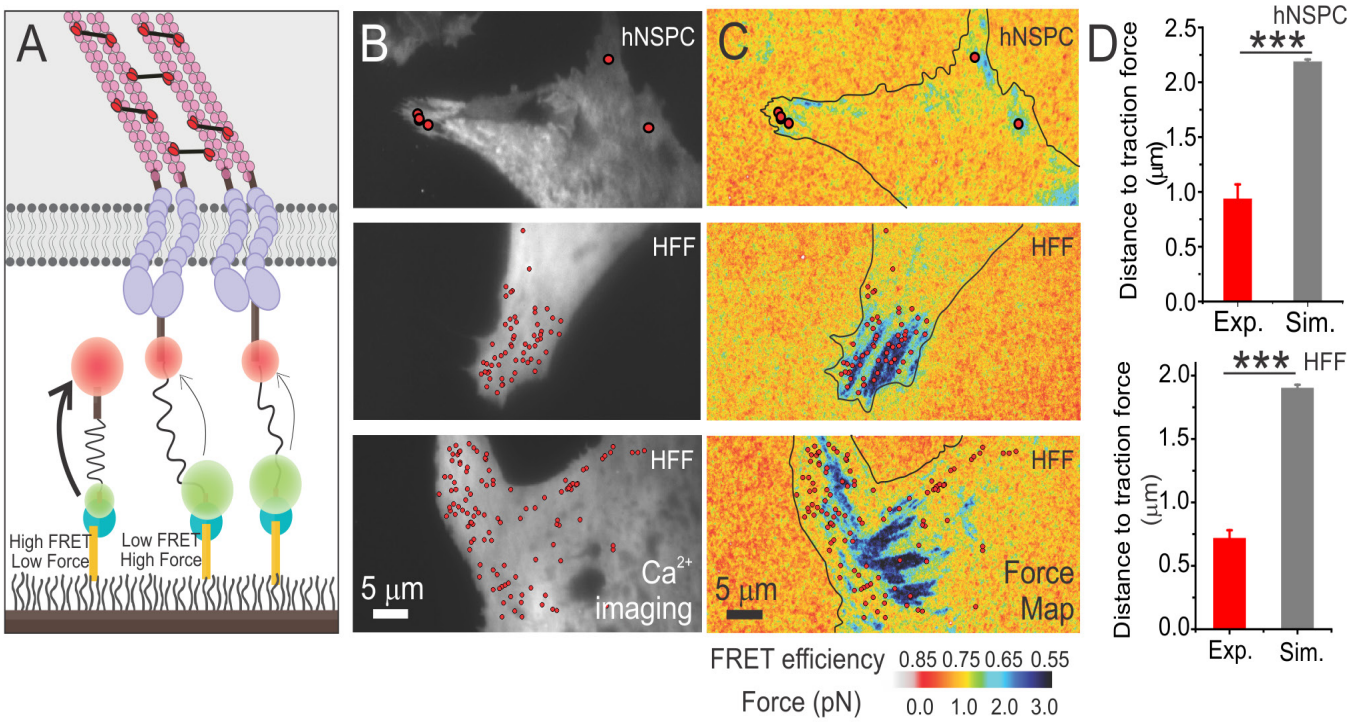

Figure 3. Piezo1 flickers localize to regions of high traction forces. A. Schematic of the Molecular Tension Sensor used for traction force imaging. The N-terminal region of the sensor (blue) is tethered to a PEG-functionalized glass coverslip. A fibronectin domain at the C-terminal end (brown) binds to the cell's integrins (purple), allowing cells to attach to the glass coverslip. An elastic spring domain bridges the two ends of the sensor and separates a FRET donor (green) and acceptor (red). Cell-generated traction forces pull the FRET pair apart, resulting in reduced FRET efficiency. The FRET index (the ratio of acceptor intensity over summed donor and acceptor intensities), serves as a measure of force; with a low FRET index indicating high force, and a high FRET index a low force. **(B)** Ca^{2+} imaging of Piezo1 flickers. Panels show resting fluorescence of cells loaded with Ca^{2+} indicator Cal-520, with overlaid red dots marking the centroid locations of Ca^{2+} flickers. The top panel shows a representative image from an hNSPC, and the middle and bottom panels show images from two HFFs. **(C)** Corresponding force maps from the same cells, overlaid with red dots marking the Ca^{2+} flicker locations. Blue denotes low FRET (high force) and red denotes high FRET (low force). The color bar in C represents FRET efficiency (top) and the average force per MTS per pixel in pN obtained from calibrated FRET-Force curves of the MTS as described in Methods. **D.** Mean distances from Piezo1 flicker localizations to the nearest traction force region for hNSPCs (top) and HFFs (bottom). Red bars show experimental data, and grey bars show simulations of 1000 random intracellular locations for each cell. hNSPCs: 66 flickers from 18 cells, *** denotes $p < 0.001$ by two-sample t-test; HFFs: 515 flickers from 9 cells, *** denotes $p < 0.001$ by two-sample t-test. Error bars denote standard error of the mean.

quantify the spatial relationship between traction forces and Piezo1 flickers, we calculated the distance of Piezo1 flickers to the nearest force-producing region (Fig. 3D). To determine whether the localization of Piezo1 flickers was different from chance, we simulated 1000 randomly localized Piezo1 flicker sites in each cell. We compared the distance of experimental and randomly simulated Piezo1 flicker localizations to the nearest high-force region. On average, simulated flicker localizations were situated 2.2 µm away from high-force regions whereas experimental flickers were 0.94 µm away ($p < 0.001$ by two-sample t-test). The juxtaposition of the Piezo1 flickers to cellular traction forces is consistent with the idea that proximal traction forces activate the channel.

We also imaged force maps and Ca^{2+} flickers in human foreskin fibroblasts (HFFs), a popular cell type for studying traction forces because they display large adhesions which generate high traction forces easily measurable by the MTS probe (Chang et al. 2016; Morimatsu et al. 2015, 2013). We observed Ca^{2+} flickers in HFFs similar to those in hNPSCs. To determine whether the Ca^{2+} flickers in HFFs originate from Piezo1, we knocked down the channel using shRNA targeting Piezo1. We observed a reduction in frequency as well as amplitude of signals upon Piezo1 knockdown (Fig. S1). Thus, Piezo1 contributes to Ca^{2+} flickers in HFFs. We quantified the proximity of Piezo1 flickers to force-producing adhesions as we did for hNSPCs and found that on average experimental flicker localizations were located 0.72 µm from force-producing adhesions, whereas simulated flicker localizations were located at a distance of 1.9 µm from force-producing regions ($p < 0.001$ by two-sample t-test). Together, our findings

indicate that Piezo1 flicker location is spatially correlated with traction forces.

Piezo1 molecules are widely distributed over the surface of the cell

Our observation of Piezo1 flickers occurring in the vicinity of force-producing focal adhesion zones suggests two possibilities – (i) Piezo1 channels are localized to focal adhesion zones where traction forces are transmitted to the substrate, or (ii) Piezo1 channels are present all over the cell surface, but are only activated by traction forces near force-producing adhesions. To distinguish between these possibilities we visualized the localization of Piezo1 proteins. The dearth of sensitive and specific antibodies against endogenous Piezo1 precluded immunolocalization of the native channel to answer this question. Instead, we used a knock-in reporter mouse where a tdTomato fluorescent protein is tagged to the C-terminus of the endogenous Piezo1 channel (Ranade et al. 2014). The expression of the Piezo1-tdTomato fusion protein is driven by the native Piezo1 promoter and regulatory elements; thus expression levels and patterns of the tagged channel are expected to be the same as that of endogenous channels. We immunostained endogenous Piezo1-tdTomato channels in mNSPCs with an anti-RFP antibody and observed channels distributed all over the cell surface (Fig. 4A).

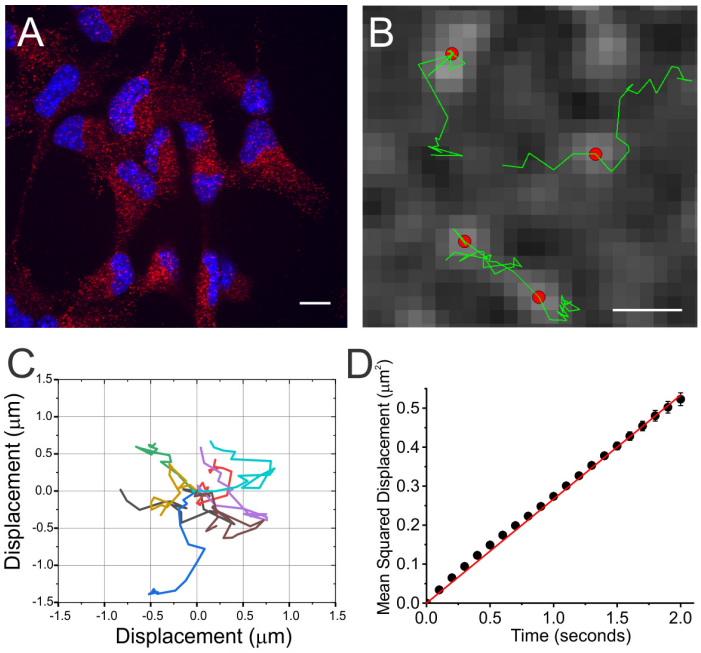

Figure 4. Piezo1 molecules are mobile in the plasma membrane. A. Single Confocal slice image at the cell-coverslip bottom surface of mNSPCs harvested from Piezo1-tdTomato reporter mice immunostained with an anti-RFP antibody (red) and Hoechst nuclear stain (blue). Note the widespread distribution of Piezo1-tdTomato channels across the cell membrane. Scale bar = 10 μm. **B.** Tracking of Piezo1-tdTomato channel puncta imaged at 10 fps in live mNSPCs reveals motility of channel puncta. The background image shows fluorescence of Piezo1-tdTomato molecules captured during a single imaging frame. Red dots mark the localizations of the molecules during that frame, and green lines depict the tracks of these molecules over several successive frames. Scale bar = 800 nm **C.** 'Flower plot' derived by overlaying the trajectories of 10 individual molecules over 1 second after normalizing their starting coordinates to the origin. **D.** Mean-squared displacement calculated from 6853 Piezo1-tdTomato tracks plotted as a function of time. Error bars represent standard error of the mean. Error bars are smaller than data symbols for most points. The data fit to a straight line with a slope corresponding to a 2D diffusion coefficient of 0.067 $\mu m^2/s$. R^2 for linear fit to data is 0.99.

Piezo1 molecules are mobile in the plasma membrane

Imaging of the tdTomato moiety in live mNSPCs by TIRF microscopy further revealed that individual Piezo1 puncta are mobile in the plasma membrane (Fig. 4B). We tracked mobile tdTomato-tagged Piezo1 channel puncta in the plasma membrane in images captured every 100 ms with TIRFM using custom-written single particle tracking scripts (See Methods) to build trajectories of individual Piezo1 puncta (Fig. 4B). Fig. 4C shows the tracks of 10 randomly chosen trajectories in a 'flower plot'. To obtain apparent diffusion coefficients, we plotted the Mean Squared Displacement, MSD, of 5,965 tracks. The slope of the MSD yields an apparent two-dimensional diffusion coefficient of = 0.067$\mu m^2/s$, which is similar to that of other membrane proteins (Marlar et al. 2014; I. F. Smith et al. 2014; "Diffusion Coefficient of Plasma Membrane Prot - Generic - BNID 114189" n.d.).

We then asked whether Piezo1 mobility is specific to the cell-substrate interface. We used lattice light-sheet imaging of Piezo1-tdTomato mNSPCs to visualize channels at both the cell-substrate interface and at the top, attachment-free, surface of the cell. We observed that Piezo1-tdTomato molecules were motile at both surfaces (Fig. S2A). In suspension cultures NSPCs form free-floating clusters known as neurospheres. We made neurospheres from Piezo1-tdTomato mNSPCs and imaged Piezo1-tdTomato molecules at the interface between NSPCs within neurospheres, which also exhibited mobility (Fig. S2B).

Thus Piezo1 mobility is observed at the cell-substrate interface, cell-cell interface, and interface-free surface of mNSPCs, indicating that mobility is a general feature of the channel. Taken together, the widespread distribution of Piezo1 channels described above and their mobility suggest that only those channels in the vicinity of focal adhesion zones are activated by local mechanical stresses produced by traction force generation.

DISCUSSION

Technical advances in Piezo1 activity measurements

Emerging evidence on the interplay of Piezo1 and the cellular cytoskeleton (Nourse and Pathak 2017) emphasizes the need for studying Piezo1 activity in native cellular conditions and in conjunction with cytoskeletal dynamics. Towards this goal, we improved our TIRFM-based Piezo1 flicker assay (Pathak et al. 2014) to provide a measure of Piezo1 activity at millisecond temporal and sub-micron spatial resolution. For this, we developed a custom-written, open-source analysis algorithm that utilizes principles from localization microscopy for the automated detection, localization, and measurement of Ca^{2+} flickers.

Our approach provides several improvements over patch clamp electrophysiology, the standard assay for Piezo1 activity. First, it does not disrupt the cellular cytoskeleton or dialyze the cell, providing a more accurate measurement of channel dynamics under native cellular conditions. Second, it allows spatial monitoring of Piezo1 activity, which is not feasible with patch clamp electrophysiology. Third, it permits examination of Piezo1 activity in response to cell-generated forces, which are orders of magnitude lower than mechanical stimuli applied in patch clamp assays.

We combined our Piezo1 flicker assay with two cell biological approaches to manipulate and measure intrinsic cellular traction forces. First, we used micropatterned substrates to constrain the shape and size of cells such that they generate a known pattern of traction forces (Singhvi et al. 1994; Chen et al. 1997; Théry 2010). Second, we used a FRET-based molecular tension sensor (MTS) (Chang et al. 2016; Morimatsu et al. 2013) to quantitatively measure cellular traction forces. Compatibility of these sensors with the Piezo1 flicker assay allowed us to measure and correlate cellular traction forces and Piezo1 activity in the same cell. Together, we provide an optimal experimental and analytical framework for examining the dynamic interplay between Piezo1 and the cytoskeleton.

Piezo1 is activated by cellular traction forces

The close proximity of Piezo1 flickers to cellular traction forces observed herein is consistent with the idea that traction forces activate the channel in hNSPCs. HFF cells, which also exhibit Piezo1-mediated flickers (Fig. S1) show a similar proximity between Piezo1 flickers and traction forces (Fig. 3), suggesting that this mechanism of Piezo1 activation is not limited to hNSPCs but may be applicable to a variety of adherent cells. These studies, together with our previous finding that the traction force inhibitor blebbistatin reversibly inhibits Piezo1 flickers (Pathak et al. 2014), establish that Piezo1 is activated by cellular traction forces.

Extracellular matrix mechanics direct stem cell differentiation (L. R. Smith, Cho, and Discher 2018), cancer pathology (Rianna, Kumar, and Radmacher 2018), and cell migration (van Helvert, Storm, and Friedl 2018). The molecular mechanisms by which mechanical properties of the matrix are transduced into the biochemical signals that regulate intracellular processes are not fully understood. The prevailing view is that cells probe the elasticity of the matrix using actively-generated traction forces, much as a person would test the elasticity of an object by pulling on it (Discher, Janmey, and Wang 2005). When presented with stiffer substrates, cells respond by generating larger traction forces; thus matrix properties are reflected in cellular contractile forces. Traction forces determine a variety of downstream signaling processes through mechanisms that are not yet fully understood. We propose that the activation of Piezo1 by cellular traction may be a key mechanism for transduction of matrix mechanical properties into intracellular Ca^{2+} signalling, which in turn regulates downstream signaling. In support of this model, stiffer substrates elicit greater Piezo1 activity than softer substrates (Pathak et al. 2014), and Piezo1 is implicated in stiffness-driven axonal guidance in embryonic development (Koser et al. 2016). Our results are consistent with similar proposals for other mechanically-activated cationic channels (Matthews et

al. 2010; Hayakawa, Tatsumi, and Sokabe 2008; Kobayashi and Sokabe 2010), suggesting that activation of cationic mechanically-activated ion channels by cell-generated forces is a fundamental mechanism in cellular mechanotransduction.

Piezo1 channels are mobile

We find that Piezo1 channels are mobile in the cell membrane (Fig. 4) with an apparent diffusion coefficient of 0.067 $\mu m^2/s$. This is within the large range of diffusion coefficients of 0.01 - 0.3 $\mu m^2/s$ measured for membrane proteins (I. F. Smith et al. 2014; Marlar et al. 2014; Pantazaka and Taylor 2011; "Diffusion Coefficient of Plasma Membrane Prot - Generic - BNID 114189" n.d.). The linear nature of the MSD plot suggests a Brownian nature to Piezo1 diffusion. However, ensemble analyses such as that used here may mask the presence of heterogeneities in single particle behavior. Moreover, while Piezo1 channels appear to diffuse readily in the plasma membrane, the restriction of flicker activity to regions of the cell that exhibit traction forces (Fig. 3) raises the possibility that active channels may be anchored. A full analysis of Piezo1 subcellular localization and dynamics is beyond the scope of this study, but is likely to provide key insights into Piezo1-mediated mechanotransduction and the interaction of the channel with its cellular environment.

How do traction forces activate Piezo1?

Several studies have proposed that Piezo1 is gated by membrane tension (Lewis and Grandl 2015; Cox et al. 2016; Syeda et al. 2016; Guo and MacKinnon 2017), and three recent cryo-EM structures of Piezo1 (Guo and MacKinnon 2017; Zhao et al. 2018; Saotome et al. 2017) support this gating mechanism. Our working model for the activation of Piezo1 flickers by traction forces is that these forces produce a local increase in membrane tension which activates Piezo1 channels in the vicinity of force-producing adhesions (Fig. 5). Whether membrane tension is a global or a local cellular parameter has been a subject of ongoing debate (Diz-Muñoz, Fletcher, and Weiner 2013). A recent study demonstrates that in intact cells -- unlike in membrane blebs -- perturbation to membrane tension can be a local event that does not necessarily propagate far (Shi et al. 2018). Taken together, our study and the work by Shi et al. provides evidence that local membrane tension induced by cytoskeletal forces can activate Piezo1. It is also possible that transient physical interactions between focal adhesion proteins (or cytoskeletal proteins) and Piezo1 may further modulate or directly activate the channel, a possibility that can be tested in future studies.

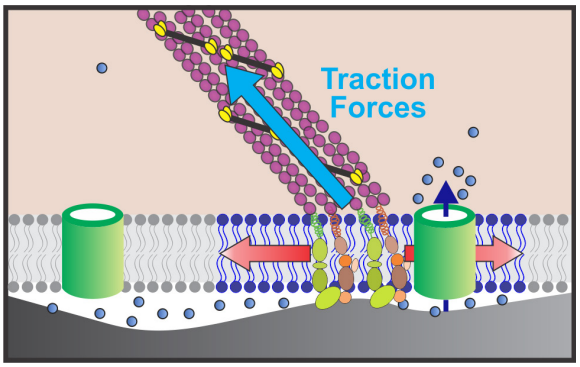

Figure 5. Working model. Traction forces (blue arrow) generated by Myosin II motors (yellow and black) along actin filaments (purple) tethered to integrin-based focal adhesion zones (green and brown) generate transient and local increases in membrane tension (depicted by blue region of lipid bilayer and red arrows) that elicit Ca^{2+} flickers from nearby Piezo1 channels (green cylinder in right part of figure). Blue dots represent Ca^{2+} ions and dark blue arrow represents Ca^{2+} influx through Piezo1. Piezo1 channels far from force-producing adhesions are not activated (green cylinder in left of figure).

An open question is whether Piezo1 flickers represent the activity of single channels or a cluster of channels, and correspondingly, whether the motile Piezo1-tdTomato puncta represent individual channels or clusters of channels that move as a unit, as has been described for IP_3 receptors (Thillaiappan et al. 2017). We observed a larger amplitude of Piezo1 flickers in larger cells, which have higher traction forces (Fig. 2), and a reduction in flicker amplitude following shRNA knockdown (Fig. S1). If flickers represent single-channel activations, then we would expect to observe changes in flicker frequency but not in amplitude under these conditions. Thus, it is likely that flickers represent the activity of a cluster of channels, with higher forces activating a larger fraction of channels in the cluster. Alternatively, the measured amplitude differences could arise from bursts of unresolved individual openings.

An emerging picture of Piezo1 mechanotransduction

Piezo1 responds on the millisecond timescale to diverse external mechanical cues such as cell

indentation (Coste et al. 2010), shear flow (Ranade et al. 2014; J. Li et al. 2014), membrane stretching (Coste et al. 2010; Lewis and Grandl 2015), substrate displacement (Poole et al. 2014), and osmotic stress (Syeda et al. 2016). Some of these mechanical stimuli impinge upon a small region of the cell, whereas others affect the cell in its entirety. How may a small number of Piezo1 channels quickly respond to mechanical cues that may strike anywhere and at any time in the cell while also transducing cell-generated traction forces that occur specifically at focal adhesion zones? We propose that -- like police patrolling a city -- mobility allows a smaller number of Piezo1 channels to explore a larger number of mechanical microdomains, and thereby respond to a diversity of mechanical cues efficiently. Whereas the electrical signal generated from Piezo1 ion flux would depolarize the cell more widely, the restricted nature of Ca^{2+} diffusion in the cytosol tightly constrains the 'chemical' signal to the vicinity of the channel. Thus, spatial localization of Piezo1 activity could serve to spatially localize biochemical signaling downstream of Piezo1, and may be a key component to its diverse physiologic roles in different cell types.

ACKNOWLEDGEMENTS
We thank Juhi Gopal, Brian Nguyen, Truc Tran, Nhu Nguyen, and Christina Le for technical assistance; Dr. Francesco Tombola, Dr. Douglas Tobias, and members of Pathak lab for discussions; and Dr. Ardem Patapoutian for the gift of Piezo1-tdTomato mice.

FUNDING
This work was supported by NIH grants R21 NS085628 (M.M.P), R37 GM048071 (I.P), F31 GM119330 (K.E.), R01 GM112998 and an HHMI Faculty Scholar Award (A.R.D.), CIRM RB5-07254 (L.A.F.) and T32 NS082174 (J.A.)

REFERENCES
Albuisson, Juliette, Swetha E. Murthy, Michael Bandell, Bertrand Coste, Hélène Louis-Dit-Picard, Jayanti Mathur, Madeleine Fénéant-Thibault, et al. 2013. "Dehydrated Hereditary Stomatocytosis Linked to Gain-of-Function Mutations in Mechanically Activated PIEZO1 Ion Channels." Nature Communications 4: 1884.

Andolfo, Immacolata, Seth L. Alper, Lucia De Franceschi, Carla Auriemma, Roberta Russo, Luigia De Falco, Fara Vallefuoco, et al. 2013. "Multiple Clinical Forms of Dehydrated Hereditary Stomatocytosis Arise from Mutations in PIEZO1." *Blood* 121 (19): 3925–35, S1–12.

Bae, Chilman, Radhakrishnan Gnanasambandam, Chris Nicolai, Frederick Sachs, and Philip A. Gottlieb. 2013. "Xerocytosis Is Caused by Mutations That Alter the Kinetics of the Mechanosensitive Channel PIEZO1." *Proceedings of the National Academy of Sciences of the United States of America* 110 (12): E1162–68.

Cahalan, Stuart M., Viktor Lukacs, Sanjeev S. Ranade, Shu Chien, Michael Bandell, and Ardem Patapoutian. 2015. "Piezo1 Links Mechanical Forces to Red Blood Cell Volume." *eLife* 4 (May). https://doi.org/10.7554/eLife.07370.

Chang, Alice C., Armen H. Mekhdjian, Masatoshi Morimatsu, Aleksandra Kirillovna Denisin, Beth L. Pruitt, and Alexander R. Dunn. 2016. "Single Molecule Force Measurements in Living Cells Reveal a Minimally Tensioned Integrin State." *ACS Nano* 10 (12). ACS Publications: 10745–52.

Chen, C. S., M. Mrksich, S. Huang, G. M. Whitesides, and D. E. Ingber. 1997. "Geometric Control of Cell Life and Death." *Science* 276 (5317): 1425–28.

Coste, Bertrand, Jayanti Mathur, Manuela Schmidt, Taryn J. Earley, Sanjeev Ranade, Matt J. Petrus, Adrienne E. Dubin, and Ardem Patapoutian. 2010. "Piezo1 and Piezo2 Are Essential Components of Distinct Mechanically Activated Cation Channels." *Science* 330 (6000): 55–60.

Coste, Bertrand, Bailong Xiao, Jose S. Santos, Ruhma Syeda, Jörg Grandl, Kathryn S. Spencer, Sung Eun Kim, et al. 2012. "Piezo Proteins Are Pore-Forming Subunits of Mechanically Activated Channels." *Nature* 483 (7388): 176–81.

Cox, Charles D., Chilman Bae, Lynn Ziegler, Silas Hartley, Vesna Nikolova-Krstevski, Paul R. Rohde, Chai-Ann Ng, Frederick Sachs, Philip A. Gottlieb, and Boris Martinac. 2016. "Removal of the Mechanoprotective Influence of the Cytoskeleton Reveals PIEZO1 Is Gated by Bilayer Tension."

Nature Communications 7 (January): 10366.
"Diffusion Coefficient of Plasma Membrane Prot - Generic - BNID 114189." n.d. Accessed April 1, 2018. http://bionumbers.hms.harvard.edu/bionumber.aspx?id=114189&ver=1.
Discher, Dennis E., Paul Janmey, and Yu-Li Wang. 2005. "Tissue Cells Feel and Respond to the Stiffness of Their Substrate." *Science* 310 (5751): 1139–43.
Diz-Muñoz, Alba, Daniel A. Fletcher, and Orion D. Weiner. 2013. "Use the Force: Membrane Tension as an Organizer of Cell Shape and Motility." *Trends in Cell Biology* 23 (2): 47–53.
Dupont, Sirio, Leonardo Morsut, Mariaceleste Aragona, Elena Enzo, Stefano Giulitti, Michelangelo Cordenonsi, Francesca Zanconato, et al. 2011. "Role of YAP/TAZ in Mechanotransduction." *Nature* 474 (7350): 179–83.
Ellefsen, Kyle L., Brett Settle, Ian Parker, and Ian F. Smith. 2014. "An Algorithm for Automated Detection, Localization and Measurement of Local Calcium Signals from Camera-Based Imaging." *Cell Calcium* 56 (3): 147–56.
Fotiou, Elisavet, Silvia Martin-Almedina, Michael A. Simpson, Shin Lin, Kristiana Gordon, Glen Brice, Giles Atton, et al. 2015. "Novel Mutations in PIEZO1 Cause an Autosomal Recessive Generalized Lymphatic Dysplasia with Non-Immune Hydrops Fetalis." *Nature Communications* 6 (September): 8085.
Gaub, Benjamin M., and Daniel J. Müller. 2017. "Mechanical Stimulation of Piezo1 Receptors Depends on Extracellular Matrix Proteins and Directionality of Force." *Nano Letters* 17 (3): 2064–72.
Gottlieb, Philip A., Chilman Bae, and Frederick Sachs. 2012. "Gating the Mechanical Channel Piezo1: A Comparison between Whole-Cell and Patch Recording." *Channels* 6 (4): 282–89.
Grashoff, Carsten, Brenton D. Hoffman, Michael D. Brenner, Ruobo Zhou, Maddy Parsons, Michael T. Yang, Mark A. McLean, et al. 2010. "Measuring Mechanical Tension across Vinculin Reveals Regulation of Focal Adhesion Dynamics." *Nature* 466 (7303): 263–66.
Guo, Yusong R., and Roderick MacKinnon. 2017. "Structure-Based Membrane Dome Mechanism for Piezo Mechanosensitivity." *eLife* 6 (December). https://doi.org/10.7554/eLife.33660.
Hayakawa, Kimihide, Hitoshi Tatsumi, and Masahiro Sokabe. 2008. "Actin Stress Fibers Transmit and Focus Force to Activate Mechanosensitive Channels." *Journal of Cell Science* 121 (Pt 4): 496–503.
Helvert, Sjoerd van, Cornelis Storm, and Peter Friedl. 2018. "Mechanoreciprocity in Cell Migration." *Nature Cell Biology* 20 (1): 8–20.
Holt, Brian D., Hengameh Shams, Travis A. Horst, Saurav Basu, Andrew D. Rape, Yu-Li Wang, Gustavo K. Rohde, Mohammad R. K. Mofrad, Mohammad F. Islam, and Kris Noel Dahl. 2012. "Altered Cell Mechanics from the inside: Dispersed Single Wall Carbon Nanotubes Integrate with and Restructure Actin." *Journal of Functional Biomaterials* 3 (2): 398–417.
Hung, Wei-Chien, Jessica R. Yang, Christopher L. Yankaskas, Bin Sheng Wong, Pei-Hsun Wu, Carlos Pardo-Pastor, Selma A. Serra, et al. 2016. "Confinement Sensing and Signal Optimization via Piezo1/PKA and Myosin II Pathways." *Cell Reports* 15 (7): 1430–41.
Kobayashi, Takeshi, and Masahiro Sokabe. 2010. "Sensing Substrate Rigidity by Mechanosensitive Ion Channels with Stress Fibers and Focal Adhesions." *Current Opinion in Cell Biology* 22 (5): 669–76.
Koser, David E., Amelia J. Thompson, Sarah K. Foster, Asha Dwivedy, Eva K. Pillai, Graham K. Sheridan, Hanno Svoboda, et al. 2016. "Mechanosensing Is Critical for Axon Growth in the Developing Brain." *Nature Neuroscience* 19 (12): 1592–98.
Lewis, Amanda H., and Jörg Grandl. 2015. "Mechanical Sensitivity of Piezo1 Ion Channels Can Be Tuned by Cellular Membrane Tension." *eLife* 4 (December). https://doi.org/10.7554/eLife.12088.
Li, Chouyang, Simin Rezania, Sarah Kammerer, Armin Sokolowski, Trevor Devaney, Astrid Gorischek, Stephan Jahn, et al. 2015. "Piezo1 Forms Mechanosensitive Ion Channels in the Human MCF-7 Breast Cancer Cell Line." *Scientific Reports* 5 (February): 8364.
Li, Jing, Bing Hou, Sarka Tumova, Katsuhiko Muraki, Alexander Bruns, Melanie J. Ludlow, Alicia Sedo, et al. 2014. "Piezo1 Integration of Vascular Architecture with Physiological Force." *Nature* 515 (7526): 279–82.
Lukacs, Viktor, Jayanti Mathur, Rong Mao, Pinar Bayrak-Toydemir, Melinda Procter, Stuart M. Cahalan, Helen J. Kim, et al. 2015. "Impaired PIEZO1 Function in Patients with a Novel Autosomal

Recessive Congenital Lymphatic Dysplasia." *Nature Communications* 6 (September): 8329.
Marlar, Saw, Eva C. Arnspang, Gitte A. Pedersen, Jennifer S. Koffman, and Lene N. Nejsum. 2014. "Measuring Localization and Diffusion Coefficients of Basolateral Proteins in Lateral versus Basal Membranes Using Functionalized Substrates and kICS Analysis." *Biochimica et Biophysica Acta* 1838 (10): 2404–11.
Matthews, Benjamin D., Charles K. Thodeti, Jessica D. Tytell, Akiko Mammoto, Darryl R. Overby, and Donald E. Ingber. 2010. "Ultra-Rapid Activation of TRPV4 Ion Channels by Mechanical Forces Applied to Cell Surface β1 Integrins." *Integrative Biology* 2 (9). Royal Society of Chemistry: 435–42.
McHugh, Brian J., Amanda Murdoch, Christopher Haslett, and Tariq Sethi. 2012. "Loss of the Integrin-Activating Transmembrane Protein Fam38A (Piezo1) Promotes a Switch to a Reduced Integrin-Dependent Mode of Cell Migration." *PloS One* 7 (7): e40346.
Miyamoto, Tatsuya, Tsutomu Mochizuki, Hiroshi Nakagomi, Satoru Kira, Masaki Watanabe, Yasunori Takayama, Yoshiro Suzuki, Schuichi Koizumi, Masayuki Takeda, and Makoto Tominaga. 2014. "Functional Role for Piezo1 in Stretch-Evoked Ca^{2+} Influx and ATP Release in Urothelial Cell Cultures." *The Journal of Biological Chemistry* 289 (23): 16565–75.
Morimatsu, Masatoshi, Armen H. Mekhdjian, Arjun S. Adhikari, and Alexander R. Dunn. 2013. "Molecular Tension Sensors Report Forces Generated by Single Integrin Molecules in Living Cells." *Nano Letters* 13 (9): 3985–89.
Morimatsu, Masatoshi, Armen H. Mekhdjian, Alice C. Chang, Steven J. Tan, and Alexander R. Dunn. 2015. "Visualizing the Interior Architecture of Focal Adhesions with High-Resolution Traction Maps." *Nano Letters* 15 (4). ACS Publications: 2220–28.
Nourse, Jamison L., and Medha M. Pathak. 2017. "How Cells Channel Their Stress: Interplay between Piezo1 and the Cytoskeleton." *Seminars in Cell & Developmental Biology* 71 (November): 3–12.
Pantazaka, Evangelia, and Colin W. Taylor. 2011. "Differential Distribution, Clustering, and Lateral Diffusion of Subtypes of the Inositol 1,4,5-Trisphosphate Receptor." *The Journal of Biological Chemistry* 286 (26): 23378–87.
Parker, Kevin Kit, Amy Lepre Brock, Cliff Brangwynne, Robert J. Mannix, Ning Wang, Emanuele Ostuni, Nicholas A. Geisse, Josephine C. Adams, George M. Whitesides, and Donald E. Ingber. 2002. "Directional Control of Lamellipodia Extension by Constraining Cell Shape and Orienting Cell Tractional Forces." *FASEB Journal: Official Publication of the Federation of American Societies for Experimental Biology* 16 (10): 1195–1204.
Pathak, Medha M., Jamison L. Nourse, Truc Tran, Jennifer Hwe, Janahan Arulmoli, Dai Trang T. Le, Elena Bernardis, Lisa A. Flanagan, and Francesco Tombola. 2014. "Stretch-Activated Ion Channel Piezo1 Directs Lineage Choice in Human Neural Stem Cells." *Proceedings of the National Academy of Sciences of the United States of America* 111 (45): 16148–53.
Poole, Kate, Regina Herget, Liudmila Lapatsina, Ha-Duong Ngo, and Gary R. Lewin. 2014. "Tuning Piezo Ion Channels to Detect Molecular-Scale Movements Relevant for Fine Touch." *Nature Communications* 5 (March): 3520.
Ranade, Sanjeev S., Zhaozhu Qiu, Seung-Hyun Woo, Sung Sik Hur, Swetha E. Murthy, Stuart M. Cahalan, Jie Xu, et al. 2014. "Piezo1, a Mechanically Activated Ion Channel, Is Required for Vascular Development in Mice." *Proceedings of the National Academy of Sciences of the United States of America* 111 (28): 10347–52.
Retailleau, Kevin, Fabrice Duprat, Malika Arhatte, Sanjeev Sumant Ranade, Rémi Peyronnet, Joana Raquel Martins, Martine Jodar, et al. 2015. "Piezo1 in Smooth Muscle Cells Is Involved in Hypertension-Dependent Arterial Remodeling." *Cell Reports* 13 (6): 1161–71.
Rianna, Carmela, Prem Kumar, and Manfred Radmacher. 2018. "The Role of the Microenvironment in the Biophysics of Cancer." *Seminars in Cell & Developmental Biology* 73 (January): 107–14.
Rode, Baptiste, Jian Shi, Naima Endesh, Mark J. Drinkhill, Peter J. Webster, Sabine J. Lotteau, Marc A. Bailey, et al. 2017. "Piezo1 Channels Sense Whole Body Physical Activity to Reset Cardiovascular Homeostasis and Enhance Performance." *Nature Communications* 8 (1): 350.
Rodriguez, Alex, and Alessandro Laio. 2014. "Clustering by Fast Search and Find of Density Peaks." *Science* 344 (6191). American Association for the Advancement of Science: 1492–96.

Saotome, Kei, Swetha E. Murthy, Jennifer M. Kefauver, Tess Whitwam, Ardem Patapoutian, and Andrew B. Ward. 2017. "Structure of the Mechanically Activated Ion Channel Piezo1." *Nature*, December. https://doi.org/10.1038/nature25453.

Shi, Zheng, Zachary T. Graber, Tobias Baumgart, Howard A. Stone, and Adam E. Cohen. 2018. "Cell Membranes Resist Flow." *bioRxiv*. https://doi.org/10.1101/290643.

Singhvi, R., A. Kumar, G. P. Lopez, G. N. Stephanopoulos, D. I. Wang, G. M. Whitesides, and D. E. Ingber. 1994. "Engineering Cell Shape and Function." *Science* 264 (5159): 696–98.

Smith, Ian F., Divya Swaminathan, George D. Dickinson, and Ian Parker. 2014. "Single-Molecule Tracking of Inositol Trisphosphate Receptors Reveals Different Motilities and Distributions." *Biophysical Journal* 107 (4): 834–45.

Smith, Lucas R., Sangkyun Cho, and Dennis E. Discher. 2018. "Stem Cell Differentiation Is Regulated by Extracellular Matrix Mechanics." *Physiology* 33 (1): 16–25.

Spier, Isabel, Martin Kerick, Dmitriy Drichel, Sukanya Horpaopan, Janine Altmüller, Andreas Laner, Stefanie Holzapfel, et al. 2016. "Exome Sequencing Identifies Potential Novel Candidate Genes in Patients with Unexplained Colorectal Adenomatous Polyposis." *Familial Cancer* 15 (2): 281–88.

Stabley, Daniel R., Carol Jurchenko, Stephen S. Marshall, and Khalid S. Salaita. 2011. "Visualizing Mechanical Tension across Membrane Receptors with a Fluorescent Sensor." *Nature Methods* 9 (1): 64–67.

Suchyna, Thomas M., Vladislav S. Markin, and Frederick Sachs. 2009. "Biophysics and Structure of the Patch and the Gigaseal." *Biophysical Journal* 97 (3): 738–47.

Syeda, Ruhma, Maria N. Florendo, Charles D. Cox, Jennifer M. Kefauver, Jose S. Santos, Boris Martinac, and Ardem Patapoutian. 2016. "Piezo1 Channels Are Inherently Mechanosensitive." *Cell Reports* 17 (7): 1739–46.

Tan, John L., Joe Tien, Dana M. Pirone, Darren S. Gray, Kiran Bhadriraju, and Christopher S. Chen. 2003. "Cells Lying on a Bed of Microneedles: An Approach to Isolate Mechanical Force." *Proceedings of the National Academy of Sciences of the United States of America* 100 (4): 1484–89.

Théry, Manuel. 2010. "Micropatterning as a Tool to Decipher Cell Morphogenesis and Functions." *Journal of Cell Science* 123 (Pt 24): 4201–13.

Thillaiappan, Nagendra Babu, Alap P. Chavda, Stephen C. Tovey, David L. Prole, and Colin W. Taylor. 2017. "Ca2+ Signals Initiate at Immobile IP3 Receptors Adjacent to ER-Plasma Membrane Junctions." *Nature Communications* 8 (1): 1505.

Wang, Ning, Emanuele Ostuni, George M. Whitesides, and Donald E. Ingber. 2002. "Micropatterning Tractional Forces in Living Cells." *Cell Motility and the Cytoskeleton* 52 (2): 97–106.

Wang, Shengpeng, Ramesh Chennupati, Harmandeep Kaur, Andras Iring, Nina Wettschureck, and Stefan Offermanns. 2016. "Endothelial Cation Channel PIEZO1 Controls Blood Pressure by Mediating Flow-Induced ATP Release." *The Journal of Clinical Investigation* 126 (12): 4527–36.

Zarychanski, Ryan, Vincent P. Schulz, Brett L. Houston, Yelena Maksimova, Donald S. Houston, Brian Smith, Jesse Rinehart, and Patrick G. Gallagher. 2012. "Mutations in the Mechanotransduction Protein PIEZO1 Are Associated with Hereditary Xerocytosis." *Blood* 120 (9): 1908–15.

Zhao, Qiancheng, Heng Zhou, Shaopeng Chi, Yanfeng Wang, Jianhua Wang, Jie Geng, Kun Wu, et al. 2018. "Structure and Mechanogating Mechanism of the Piezo1 Channel." *Nature* 554 (7693): 487–92.

Supplemental Figures

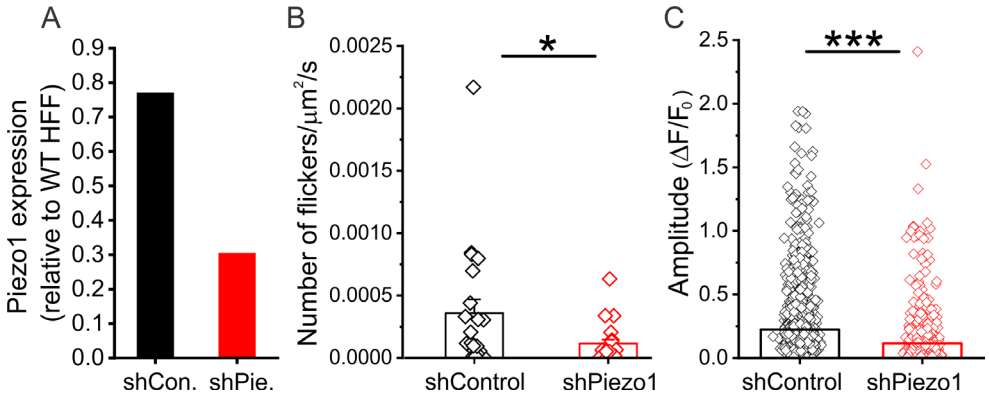

Figure S1. shRNA knockdown of Piezo1 in HFFs reduces Piezo1 flickers. A. Piezo1 expression in HFFs transfected with non-silencing Control or Piezo1 shRNA constructs. **B.** Frequency of Ca^{2+} flickers in shControl- and shPiezo1-transfected HFF cells. Bar graph shows mean frequency (3.6×10^{-4} events/μm^2/second obtained from 21 videos for shControl; and 1.1×10^{-4} from 22 videos for shPiezo1). Each point represents frequency of videos in a single video. * denotes $p = 0.036$ by two-sample t-test. **C.** Amplitude of Ca^{2+} flickers in shControl- and shPiezo1-transfected HFF cells. Bar graphs represent mean amplitude (0.22 for shControl; 0.12 from shPiezo1) calculated from 2133 flickers for shControl and 1042 flickers from shPiezo1. *** denotes $p < 0.001$ by two-sample t-test.

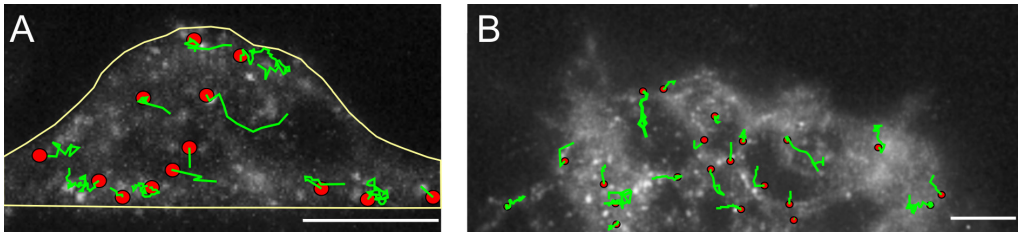

Figure S2. Lattice light-sheet imaging shows Piezo1 channels are motile on all surfaces of the cell. Imaging of Piezo1-tdTomato protein in mNSPCs by lattice lightsheet microscopy in a single cell **(A)** and in neurospheres **(B)**. The background images show a maximum intensity projection of the entire movie. Red dots and green tracks mark trajectories of a subset of single puncta in contiguous frames. Yellow lines in A depict the outline of `the cell imaged. Images were acquired every 50 ms. Scale bars = 10 μm.

Materials and Methods

Cell Culture

hNSPC Culture. Brain-derived fetal hNSPC cultures (SC27) were isolated from the cerebral cortex of a male fetus of 23-wk gestational age and were maintained as previously described (Pathak et al. 2014). Briefly, undifferentiated cells were grown as adherent cultures on fibronectin (Fisher Scientific)-coated flasks in basal medium containing DMEM/F12 (GIBCO), 20% BIT-9500 (Stem Cell Technologies), and 1% antibiotic/antimycotic (Invitrogen) supplemented with the following growth factors: 40 ng/mL EGF (BD Biosciences), 40 ng/mL FGF (BD Biosciences), and 40 ng/mL PDGF (Peprotech). hNSPCs were passaged approximately every 5-7 days using Cell Dissociation Buffer (Invitrogen) and split 1:2. Cells were used at passages P10–22. Informed written consent was obtained for all human subjects.

mNSPC Culture. NSPCs from cerebral cortices of embryonic mice (age E12.5) expressing a C-terminal fusion of Piezo1 with tdTomato (Piezo-tdTomato) (Ranade et al. 2014) were cultured as neurospheres as described previously (Nourse et al. 2014). Piezo1-tdTomato reporter mice were a gift from A. Patapoutian. mNSPC growth medium consisted of: High glucose Dulbecco's modified Eagle's medium (all reagents from Life Technologies unless otherwise noted), 1x B27, 1x N2, 1 mM sodium pyruvate, 2 mM glutamine, 1 mM N-acetylcysteine (Sigma Aldrich), 20 ng/ml epidermal growth factor (EGF) (BD Biosciences), 10 ng/ml fibroblast growth factor (FGF) (BD Biosciences), and 2 μg/ml heparin (Sigma Aldrich). Cells were passaged by dissociation with Neurocult Chemical Dissociation Kit (Stem Cell Technologies). For immunostaining, NSPCs and HFF cells were plated on #1.5 glass coverslips (Warner Instruments). For live cell TIRFM imaging, mNSPCs cells were plated on #1.5 glass Mat-Tek dishes (Mat-Tek Corporation). Glass substrates were coated with 20 μg/ml laminin (Invitrogen/Life Technologies).

HFF cell culture. Human foreskin Fibroblasts (HFF-1) were purchased from ATCC (ATCC® SCRC-1041™) and cultured in medium consisted of high-glucose Dulbecco's modified Eagle's medium (all reagents from Life Technologies unless otherwise noted), 1 mM sodium pyruvate, 1x MEM-NEAA, 1% Pen/Strep, and 10% heat-inactivated FBS (Omega Scientific). Cells were passaged 1:5 with TrypLE every 4-5 days. For live cell TIRFM imaging, cells were plated on No. 1.5 glass Mat-Tek dishes (Mat-Tek Corporation) coated with 10 μg/ml human fibronectin (Corning).

Generation of micropatterned square cells. Coverslips with square micropatterns were purchased from Cytoo (https://cytoo.com/, Catalog # CYTOOchips PADO-SQRS). CYTOOchips were coated with fibronectin per manufacturer's instructions and hNSPCs were plated using a density of 1.5 x 10^4 cells/ml per manufacturer's instructions in growth media. For TIRFM Ca^{2+} imaging live cells were imaged 2-5 hours after seeding. For immunofluorescence experiments, cells were fixed with 4% paraformaldehyde in phosphate-buffered saline supplemented with 5 mM $MgCl_2$, 10 mM EGTA, 40 mg/ml sucrose, pH 7.5.

shRNA knockdown experiments.

Piezo1 knockdown experiments used inducible Dharmacon TRIPZ Lentiviral plasmids that employed shRNA containing unique microRNA-30 based hairpin design with non-silencing Control or Piezo1 specific sequences (Control (RHS7476), shPiezo (clone ID V3THS_361173) (GE Healthcare). shRNA and TurboRFP are part of a single transcript that is inducible in a Tet-On system, which enables visual assessment of shRNA expressing cells with fluorescent microscopy. The plasmid also contains a puromycin resistance gene to allow selection of plasmid containing cells. TRIPZ plasmids were introduced to the cells using Nucleofector (Amaxa® Human Dermal Fibroblasts Nucleofector® Kit, cat # VPD-1001), following manufacturer instructions. Knockdown was assessed by qRT-PCR for every transfection experiment.

Expression of shRNA and TurboRFP was induced 1 day after transfection of HFF cells with 1 μg/ml doxycycline treatment for 5-7 days. Ca^{2+} imaging by TIRFM imaging was performed on red fluorescent cells. A subset of these transfected cells were also selected with 1 μg/ml puromycin for 7-14 days to remove cells that did not receive the TRIPZ plasmids for gene expression analysis.

Gene expression analysis.
For quantitation of Piezo1 gene expression in shRNA knockdown experiments, RNA was isolated and cDNA prepared with TaqMan Gene Expression Cells-to-CT Kit (Invitrogen). qPCR was performed using TaqMan probe-based gene expression assays (UBC, assay ID # Hs_00824723_m1 and Piezo1, assay ID # Hs00207230_m1) and Taqman universal PCR master mix (Applied Biosystems). Data were collected using Applied Biosystems ViiA 7 and QuantStudio Real Time PCR System v1.2 and were analyzed by the comparative cycle threshold (C_T) method using UBC as the reference gene.

Immunofluorescence Staining.
Immunostaining was performed as previously described (Pathak et al. 2014) using the following antibodies: Rabbit anti-RFP (RFP Antibody Pre-adsorbed; Rockland, Cat# 600-401-379), 1:200 (0.95 µg/ml) and mouse anti-paxillin (clone 5H11, Millipore Cat # 05-417), 1:1000. Secondary antibodies used were Goat anti-rabbit Alexa Fluor 555 (Invitrogen Cat# A21428) and Donkey anti-mouse Alexa Fluor 488 (Invitrogen, Cat# A-21202) were used at 1:200 (0.01 mg/ml). Nuclei were stained by Hoechst 33342 (Life Technologies) at 4 µg/mL in PBS and actin filaments were stained with Phalloidin conjugated with TRITC (Sigma-Aldrich Catalog #P1951).

Imaging
Imaging Piezo1 flickers. Piezo1 flickers were detected using Ca^{2+} imaging by TIRF microscopy. Cells were loaded by incubation with 1-2 µM Cal-520 AM (AAT Bioquest Inc.) in phenol red-free DMEM/F12 (Invitrogen) for 20-30 min at 37 °C, washed three times, and incubated at room temperature for 10–15 min to allow cleavage of the AM ester. Imaging was performed at room temperature in a bath solution comprising 148 mM NaCl, 3 mM KCl, 3 mM $CaCl_2$, 2 mM $MgCl_2$, 8 mM glucose, and 10 mM HEPES (pH adjusted to 7.3 with NaOH).

For imaging Piezo1 flickers in hNSPCs in Fig. 1 and Fig. 2, movies were acquired at 100 or 200 Hz frame rate on a custom-built Spinning-Spot Shadowless TIRF microscope. Details of construction and comparison to traditional TIRF can be found in Ellefsen et al. 2015 (Ellefsen, Dynes, and Parker 2015).

Piezo1 flickers in HFFs (Fig. S1) were imaged on a motorized Olympus IX83 microscope, equipped with an automated 4-line cellTIRF illuminator and a PLAPO 60x oil immersion objective with a numerical aperture of 1.45. Mat-tek dishes of shRNA-transfected cells loaded with Cal-520 AM were first scanned using an Olympus UPLSAPO 10x objective to identify cells expressing TurboRFP. Spatial coordinates of red fluorescent cells were marked using a programmable stage (Applied Scientific Instruments). Then the objective lens and illumination were switched for TIRF imaging, and previously identified red cells were imaged for Piezo1 flicker activity. Cells were illuminated with a 488 nm laser and images were acquired with a Hamamatsu Flash v4 scientific CMOS camera at 10 ms exposure and a frame rate of 9.54 frames/second.

Imaging Piezo1 flickers and cellular traction forces in the same cell. Fabrication of Förster resonance energy transfer (FRET)-based molecular tension sensors (MTSs) to measure cellular traction forces was performed as previously described (Chang et al. 2016). The MTS is comprised of an elastic spring domain derived from spider silk, which is flanked by a covalently-bound FRET pair, Alexa 546 and Alexa 647. The N-terminus of the sensor possesses a HaloTag domain, while the C-terminal end presents the ninth and tenth type III domains of fibronectin.

Perfusion chambers (Grace Biolabs 622103) were attached to HaloLigand/PEG-functionalized coverslips. The MTS (at 0.03 mM for HFFs and 0.04 mM for hNSPCs) was added to the flow cell and incubated at room temperature for 30 min, washed with PBS twice, and passivated with 0.2% w/v Pluronic F-127 for 5 min. Flow cell channels were washed once with PBS before adding freshly dissociated cells in normal culture media and incubated at 37 °C with 5% CO_2. Cells were typically allowed to spread for 1 h before imaging and not imaged for longer than 5 h after seeding. Cells were loaded with Cal-520 AM Ca^{2+} indicator as described above and imaged in DMEM/F12 medium containing 10% FBS and 3 mM $CaCl_2$.

FRET-based traction force measurements and Piezo1 flicker measurements were performed with TIRFM on an inverted microscope (Nikon TiE) with an Apo TIRF 100x oil objective lens, NA 1.49 (Nikon). The FRET probe was excited with 532 nm (Crystalaser). Emission from Alexa 546 and Alexa 647 was separated using custom-built optics as described previously (Chang et al. 2016; Morimatsu et al. 2015). Donor and acceptor images were focused on the same camera chip. Data were acquired at 5 frames per second with an EMCCD camera (Andor iXon). Following imaging of the FRET force sensor, a motorized filter flip mount (Thor Labs) was used to switch emission filters for imaging Cal-520 Ca^{2+} indicator in the same cell. Cal-520 was excited using a 473 nm (Coherent Obis) laser and imaged at 15.29 ms exposure time.

Imaging Piezo1 diffusion with TIRFM. For Piezo1 diffusion studies in Fig. 4B-D, images were acquired on a Nikon N-STORM system built around a Nikon Eclipse Ti microscope. The imaging objective used was a Nikon 100x APO TIRF oil immersion objective (NA 1.49). Images were acquired on an Andor iXon3 electron-multiplying charge-coupled device (EMCCD) camera with an 100 ms exposure time and 160 nm/px in TIRF mode. Cells were continuously illuminated with a 561 nm laser.

Imaging Piezo1 diffusion with lattice light-sheet imaging. Lattice light-sheet imaging for Fig. S2 was performed using a custom built system as described (Ellefsen & Parker, 2018). In brief, a lattice pattern created by a custom graticule was projected through an annular aperture onto the back focal plane of a projection objective (Nikon, 40x NA 0.8 water immersion) to generate an array of Bessel beams creating an effective light sheet with a thickness of ~ 1.2 mm and extent of 50 x 25 mm. A 562 nm laser was used for fluorescence excitation of Piezo-tdTomato, and emitted light was captured by an identical, orthogonal 40x objective lens, passed through a 610 nm long-pass filter, and imaged by an Andor Zyla 4.2 sCMOS camera at a final resolution of 110nm/px.

Confocal imaging. Confocal imaging was performed on a Zeiss Confocal Spinning Disc Confocal Microscope (Zeiss) using a 63X objective with a numerical aperture of 1.40. Image stacks were acquired with 405nm, 488nm, and 561nm lasers, in intervals of 0.3 μm thickness using the AxioVision Rel 4.8 software.

Image analysis

Automated detection of Piezo1 flickers. Piezo1-mediated Ca^{2+} flickers were detected using an improved version of our published algorithm for automated detection of Ca^{2+} signals (Ellefsen et al. 2014). The new algorithm, which runs as a plug-in under the open-source image processing and analysis package Flika (https://github.com/flika-org/flika), uses a clustering algorithm (Rodriguez and Laio 2014) to group super-threshold pixels into calcium events, improving both signal detection and segregation of signals which overlap temporally or spatially.

An F/F_0 movie is generated from the original recording by subtracting the camera black level and dividing each pixel at every frame by its average value across the first ~100 frames. To remove low temporal frequency signal drift, the F/F_0 movie is temporally filtered with a high pass Butterworth filter. To standardize variance across pixels, the value of each pixel is divided by the standard deviation of the values at baseline. The noise in this 'normalized' movie is normally distributed with a mean of 0 and standard deviation of 1.

A threshold is applied to a spatially-filtered version of the 'normalized' movie to generate a binary movie. Each super-threshold pixel in this binary movie is putatively considered part of a flicker. In order to group these pixels together, we modified the clustering algorithm published by Rodriguez and Laio (Rodriguez and Laio 2014). Briefly, a density is assigned to every super-threshold pixel by counting the number of pixels in an user-defined ellipsoid centered around the pixel. Then, for every pixel, the distance to the nearest pixel with a higher density is determined. Pixels that represent the center of clusters will have both a high density and a high distance to a pixel with higher density. The user manually selects pixels exceeding a density and distance threshold as cluster centers. The algorithm then assigns every other pixel to a cluster center pixel recursively, by finding the cluster of the nearest pixel of higher density.

Once all pixels have been clustered, clusters below a user-defined size are removed.

After flickers have been identified by the clustering algorithm, the subpixel centroid of the signal is found by averaging each pixel in the 'normalized' movie over the flicker duration, and fitting a 2D Gaussian function to this average image. The peak amplitude, temporal dynamics, and frequency of signals at specific sites can be quantified, and the resulting data can be exported as Excel or csv files.

This algorithm is implemented in the puff_detect plugin for the image analysis software Flika, downloadable at https://github.com/kyleellefsen/detect_puffs. Both the puff_detect plugin and flika are open source software written in the Python programming language. Instructions for installation and use of the algorithm can be found at http://flika-org.github.io/.

Generation of cellular force maps. Analysis of FRET signals from the MTS was performed following the methodology from Morimatsu & Mekhdjian et al., Nano Letters 2015. Briefly, FRET index maps were generated by dividing the acceptor intensity *A* (background subtracted) by the sum of the acceptor and donor (*D)* intensities (also background subtracted): $FRET_i = A / (A + D)$. FRET index maps can be converted to FRET efficiency maps to extract quantitative values for force from the FRET efficiency to force calibration curve. FRET index is converted to FRET efficiency using the following equation:

$$E = (FRET_i)/(\alpha\ (\gamma\text{-}FRET_i\ \gamma+FRET_i\ )\ )$$

Where E is the FRET efficiency, $FRET_i$ is the FRET index, α is the fraction of donor-labeled sensors that have an acceptor, and γ is a factor that accounts for differences in donor and acceptor quantum yield. Both α and γ are experimentally determined (Morimatsu et al., Nano Letters 2015). The FRET efficiency is converted to force using a phenomenological fit (Chang et al., ACS Nano 2016) to the FRET-force response of the $(GPGGA)_8$ linker (Grashoff et al., Nature 2010).

Calculation of distance from Piezo1 flicker localization to nearest force-producing region. Force-generating regions were determined by blurring the force maps with a Gaussian filter. Regions in which the pixel intensity was below 75% of maximum intensity were considered force generating. Distances from each flicker centroid to the nearest force generating region were measured. To calculate the average distance to the nearest force generating region in each cell, the outline of each cell was manually traced, 1000 points were randomly selected inside this outline, and the distance to the nearest force generating region was measured.

Piezo1 particle tracking. TIRFM image stacks were processed in order to determine the location of Piezo1-tdTomato puncta in each frame. Each frame was spatially bandpass filtered by taking the difference of Gaussians, an image processing algorithm that enhances a band of spatial frequencies--in this case, around the size of the particles. The spatially filtered movie was then thresholded using a manually determined threshold, yielding a binary movie. Spatially contiguous pixels above threshold were grouped together and considered a single particle. The centroid for each particle was determined by fitting a 2D Gaussian function to each particle, yielding a centroid with subpixel precision. The initial x, y values for the fit were set to be the center of mass of the binary pixels in the particle. Any localizations within consecutive frames that were within three pixels of each other were assumed to arise from the same particle. These localizations were linked over time to generate particle tracks.

Piezo1-tdTomato puncta in single mNSPCs and in neurospheres imaged with lattice-lightsheet microscopy were tracked using the 2D/3D particle tracker which is part of the MosaicSuite ImageJ plugin (Sbalzarini and Koumoutsakos 2005). Only particles larger than a radius of 7 pixels were considered.

References.

Chang, Alice C., Armen H. Mekhdjian, Masatoshi Morimatsu, Aleksandra Kirillovna Denisin, Beth L. Pruitt, and Alexander R. Dunn. 2016. "Single Molecule Force Measurements in Living Cells Reveal a Minimally Tensioned Integrin State." *ACS Nano* 10 (12). ACS Publications: 10745–52.

Ellefsen, Kyle L., Joseph L. Dynes, and Ian Parker. 2015. "Spinning-Spot Shadowless TIRF Microscopy." *PloS One* 10 (8): e0136055.

Ellefsen, Kyle L., and Ian Parker. 2018. "Dynamic Ca2+ Imaging with a Simplified Lattice Light-Sheet

Microscope: A Sideways View of Subcellular Ca2+ Puffs." *Cell Calcium* 71 (May): 34–44.

Ellefsen, Kyle L., Brett Settle, Ian Parker, and Ian F. Smith. 2014. "An Algorithm for Automated Detection, Localization and Measurement of Local Calcium Signals from Camera-Based Imaging." *Cell Calcium* 56 (3): 147–56.

Morimatsu, Masatoshi, Armen H. Mekhdjian, Alice C. Chang, Steven J. Tan, and Alexander R. Dunn. 2015. "Visualizing the Interior Architecture of Focal Adhesions with High-Resolution Traction Maps." *Nano Letters* 15 (4). ACS Publications: 2220–28.

Nourse, J. L., J. L. Prieto, A. R. Dickson, J. Lu, M. M. Pathak, F. Tombola, M. Demetriou, A. P. Lee, and L. A. Flanagan. 2014. "Membrane Biophysics Define Neuron and Astrocyte Progenitors in the Neural Lineage." *Stem Cells* 32 (3): 706–16.

Pathak, Medha M., Jamison L. Nourse, Truc Tran, Jennifer Hwe, Janahan Arulmoli, Dai Trang T. Le, Elena Bernardis, Lisa A. Flanagan, and Francesco Tombola. 2014. "Stretch-Activated Ion Channel Piezo1 Directs Lineage Choice in Human Neural Stem Cells." *Proceedings of the National Academy of Sciences of the United States of America* 111 (45): 16148–53.

Ranade, Sanjeev S., Zhaozhu Qiu, Seung-Hyun Woo, Sung Sik Hur, Swetha E. Murthy, Stuart M. Cahalan, Jie Xu, et al. 2014. "Piezo1, a Mechanically Activated Ion Channel, Is Required for Vascular Development in Mice." *Proceedings of the National Academy of Sciences of the United States of America* 111 (28): 10347–52.

Rodriguez, Alex, and Alessandro Laio. 2014. "Clustering by Fast Search and Find of Density Peaks." *Science* 344 (6191). American Association for the Advancement of Science: 1492–96.

Sbalzarini, I. F., and P. Koumoutsakos. 2005. "Feature Point Tracking and Trajectory Analysis for Video Imaging in Cell Biology." *Journal of Structural Biology* 151 (2): 182–95.